The Meteoritical Society

Meteoritics & Planetary Science 50, Nr 6, 1139–1155 (2015)
doi: 10.1111/maps.12457

Accessory and opaque minerals in impact melt rocks of the Boltysh structure, Ukraine

E. P. GUROV*, S. B. SHEKHUNOVA, and V. V. PERMYAKOV

Institute of Geological Sciences, National Academy of Sciences of Ukraine, Gontchara Str., 55b, Kiev, Ukraine
*Corresponding author. E-mail: yevgeniy.gurov@gmail.com

(Received 12 August 2013; revision accepted 09 March 2015)

Abstract–Electron microprobe analyses of accessory and opaque minerals from the impact melt rocks of the Boltysh structure, in the central part of the Ukrainian Shield, are presented in this report. Our study establishes a variety of minerals represented by native metals, alloys, oxides, sulfides, phosphates, and silicates, formed during several stages of cooling and solidification of the thick impact melt sheet. Baddeleyite was determined to be the earliest high-temperature mineral to occur in the impact melt rocks. Iron and titanium oxides crystallized earlier or simultaneously with the microliths of orthopyroxene and feldspars. High concentrations of TiO_2, Al_2O_3, and Cr_2O_3 were identified in some hematite varieties. Cu- and Ni-bearing pyrrhotites occur in impact melt rocks with a glassy matrix. Native metals—copper, platinum, and silver—were likely formed due to the hydrothermal alteration of the upper unit of the impact melt sheet. Zircon is the only accessory mineral found in impact melt rocks that is preserved from the basement granites of the Boltysh structure.

INTRODUCTION

The Boltysh impact structure, a circular depression about 24 km in diameter and nearly 1 km in morphologic depth, was formed in the Precambrian granites and gneisses of the Ukrainian Shield (Masaitis 1973; Golubev et al. 1974; Yurk et al. 1975) (Fig. 1). The crater was formed 65.82 ± 0.74 Ma ago and was identified as another end-Cretaceous impact structure (Kelley and Gurov 2002; Jourdan et al. 2012). Subsequent investigations suggested that Boltysh predated Chicxulub by ~2–5 kyr (Jolley et al. 2010). The impactite sequence of the Boltysh crater is composed of impact melt rocks, impact melt-bearing breccias (suevites), and other types of clastic breccias. The crater is filled with postimpact Tertiary sediments up to 550 m thick. Quaternary deposits of up to 20–30 m thick and postimpact sediments ensured the complete preservation of the impact rock complex within the structure, including the unique annular sheet of impact melt rocks (Valter and Ryabenko 1977; Masaitis et al. 1980; Gurov and Gurova 1991; Gurov et al. 2006).

The structure of the melt sheet and the composition of impact melt rocks, their petrography, mineralogy, and geochemistry have been described in the literature (e.g., Valter and Ryabenko 1977; Masaitis et al. 1980; Gurov et al. 1986; Grieve et al. 1987; Gurov and Gurova 1991). Although the rock-forming minerals of the Boltysh impact melt rocks were studied soon after the discovery of the impact origin of the crater (Yurk et al. 1975; Valter and Ryabenko 1977; Masaitis et al. 1980; Grieve et al. 1987), accessory minerals have not yet been investigated. Thus, the aim of this paper is (1) to study the accessory and opaque minerals from impact melt rocks of the Boltysh structure and (2) to gain new insights into the impact melt petrology from the composition and distribution of these accessory phases.

Our investigations discovered a wide variety of minerals, including native metals, oxides, sulfides, phosphates, and others. A systematic characterization of these phases provides a better understanding of the processes of impact melt cooling and solidification.

IMPACT MELT ROCKS OF THE BOLTYSH STRUCTURE

The Boltysh is a complex impact crater with a central uplift that is 4 km in diameter and up to 600 m

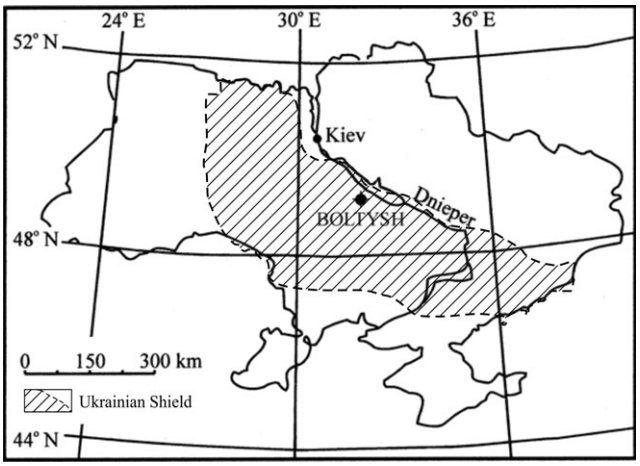

Fig. 1. Location of the Boltysh impact structure at the NE slope of the Ukrainian Shield (shaded area), Ukraine.

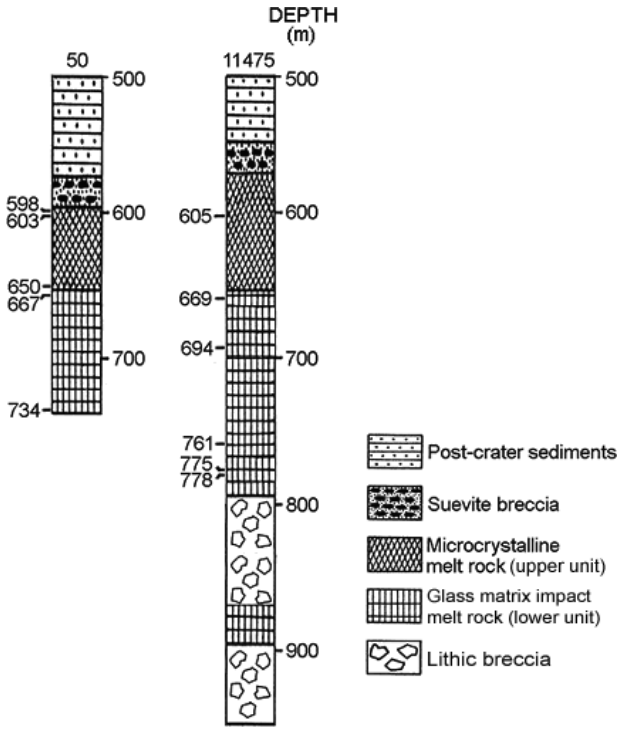

Fig. 2. Stratigraphic columns of the impact melt rocks, suevites and overlying postimpact sediments of drill holes 50, located 4.9 km to the SW from the center of the Boltysh structure, and 11475, located 3.5 km to the SW from the center. The depth of samples studied is shown to the left of the columns.

in height above the structural crater floor. The central uplift is surrounded by a deep inner crater that is ~12 km wide and up to 1 km deep. Impact melt filled the inner crater around the central uplift, forming an annular sheet of impact melt rocks. The subhorizontal surface of the sheet is considered evidence that the high-temperature mobile melt formed the lake in the deepest part of the structure immediately after its formation. An interrupted layer of clastic melt-bearing breccia (suevites) up to 20–30 m thick overlies the surface of the melt sheet. Furthermore, impact melt rocks are overlain by postimpact sediments up to 550 m thick in the deepest part of the structure (Masaitis et al. 1980; Gurov and Gurova 1991; Gurov et al. 2003).

The melt sheet is 11–12 km in diameter, and based on drill hole 11475 located 3.5 km SW of the crater's center, it reaches a thickness of 219 m. The thickness of the drilled part of the melt sheet is 142.5 m in drill hole 50, which is 4.9 km SW of the crater's center, while its complete thickness here was estimated at 155–160 m (Gurov and Gurova 1991; Gurov et al. 2011). Several drill holes, including hole 42 drilled in 2008 (Jolley et al. 2010), stripped only the upper part of the impact melt sheet.

According to several studies (Masaitis et al. 1980; Grieve et al. 1987; Gurov and Gurova 1991; Gurov et al. 2011), two main units of impact melt rocks can be distinguished in the impact melt sheet of the Boltysh structure (Fig. 2). Hialine impact melt rocks with a glassy matrix and microliths of feldspar and orthopyroxene compose the lower unit of the melt sheet (Fig. 3a) at the intervals of 792–657 m in drill hole 11475 and 736–653 m in drill hole 50 (Valter and Ryabenko 1977; Masaitis et al. 1980; Gurov et al. 1986; Grieve et al. 1987; Gurov and Gurova 1991). Microcrystalline impact melt rocks with microliths of feldspars and completely chloritized pyroxene (Fig. 3b) form the upper unit of the impact melt sheet at intervals from 657 m to its surface at 573 m in drill hole 11475, and from 653 m to 594 m in drill hole 50.

Within the lower, glassy (hemihyaline) unit feldspar microliths up to 0.7 mm in length are composed of zoned plagioclase, with composition ranging from labradorite ($Ab_{45}An_{50}Or_5$) in their central parts to andesine ($Ab_{55}An_{40}Or_5$) in the outer zones. Late tabular and skeletal microliths of feldspar are represented by barium-bearing sanidine ($Or_{55–65}Ab_{28–38}An_{4–5}Cn_{2–3}$). A similarly composed feldspar also forms overgrowths of the swallow-tail structures of the microliths (Gurov et al. 2011). Orthopyroxene forms up to three discrete generations in the impact melt rocks. The earliest generation consists of prismatic zoned microliths up to 1.0–1.5 mm in length with hypersthene $En_{65–70}$ in their cores and $En_{45–55}$ in the peripheral zones. Orthopyroxene of the second generation forms thin prismatic and skeletal microliths of ferrohypersthene $En_{30–36}$. The latest pyroxene generation is represented by hair-like trichites and rare micrometer-size crystallites of eulite $En_{15–30}$. The matrix of the impact melt rocks is either fresh or made of glass with cryptocrystalline skeletal aggregates of sanidine (Gurov et al. 2011).

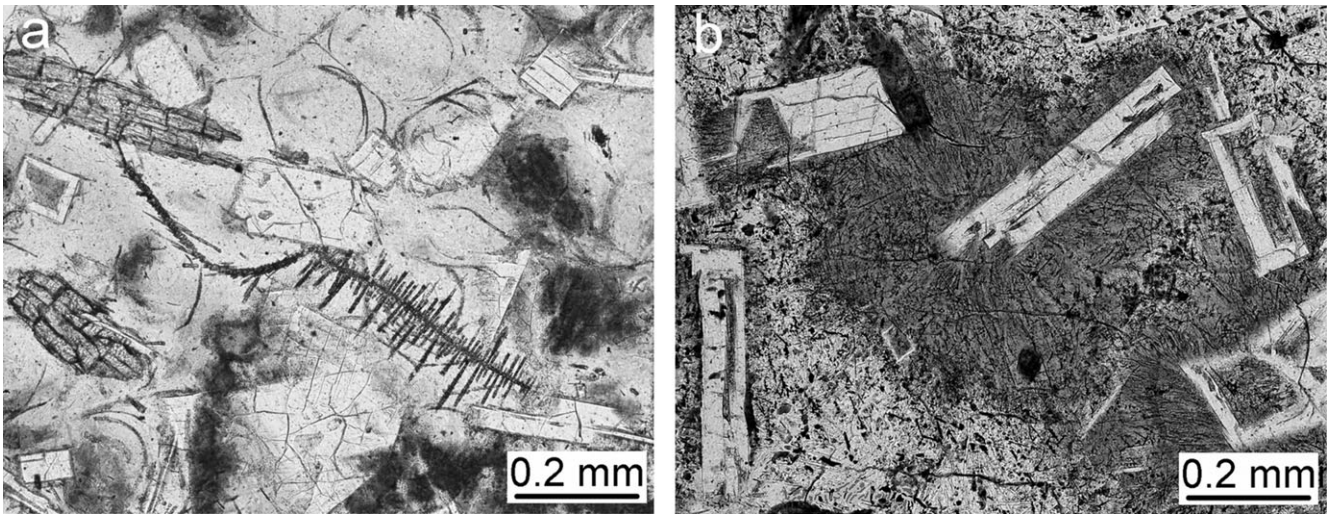

Fig. 3. Microphotographs of the main types of the impact melt rocks of the Boltysh structure. a) The glassy matrix impact melt rock of the lower unit of the melt sheet. The prismatic microliths of feldspars (white) and hypersthene (dark gray in the left part of the image) occur in the glassy matrix. In the central part if the image the skeletal growth of ferrohypersthene. Dark gray areas in low and left parts of image represent a devitrification of the glassy matrix (drill hole 11475, 761 m, plan-polarized light). b) The microcrystalline impact melt rock of the upper unit of the melt sheet. Prismatic and hollow microliths of feldspars are surrounded by the spherulitic groundmass (drill hole 50, 603 m, plan-polarized light).

The microcrystalline impact melt rocks of the upper unit contain microliths of feldspars and segregations of chlorite, which have completely replaced microliths of pyroxene. The composition of weakly zoned feldspar microliths is from ($Ab_{43–50}An_{55–47}Or_2$) in the inner zones to ($Ab_{61–66}An_{35–32}Or_{2–6}$) in their marginal parts. Late microliths of sanidine ($Or_{55–57}Ab_{40–42}An_{1–3}Cn_{1–2}$) show tabular and skeletal growth and an average crystal length of 0.1–0.3 mm. Chlorite completely replaces microliths of pyroxene and forms reaction coronas around ballen silica. The impact melt rock matrix is composed of cryptocrystalline intergrowths of feldspar and quartz, forming granophyric textures; glass is absent in this rock type. As supposed by Gurov et al. (2006, 2011), the complete chloritization of pyroxene, as well as the crystalline structure of the matrix of the melt rocks of the upper horizon, are likely caused by interaction with meteoric water and associated hydrothermal alteration.

The target rocks of the Boltysh structure are Proterozoic granites and biotite gneisses with a volumetric ratio of about 5:1 (Masaitis et al. 1980; Gurov et al. 1986). The composition of the impact melt rocks of the Boltysh structure is similar to that of its preimpact target rocks and is homogeneous across the whole section of the sheet in boreholes 50 and 11475. Some compositional differences in the composition of the lower and upper melt rock units are expressed by the degree of oxidation/reduction of Fe in those rocks: while the ratio Fe_2O_3/FeO in target rocks is 0.50, it decreases to 0.32 in the lower unit and rises to 1.37 (up to 2.10 in some samples) in the upper unit (Gurov et al. 1986, 2006).

The search for potential projectile traces and attempts to determine its type have been made by several previous researchers (Valter and Ryabenko 1977; Gurov et al. 1986; Grieve et al. 1987; McDonald et al. 2009). The enrichment of impact melt rocks in Ni and Cr to about 10–15 times and Co 2–4 times relative to their contents in the target rocks suggested a stony composition of the Boltysh impactor (Gurov et al. 1986, 2006; Grieve et al. 1987). Furthermore, the slight enrichment of the platinum-group elements (PGE) Ir and Ru in three samples of impact melt rocks from drill hole 50 suggested a minor chondritic contribution (McDonald et al. 2009).

SAMPLES AND ANALYTICAL TECHNIQUES

Representative samples derived from the two impact melt rock units present at the Boltysh impact structure were selected for a detailed microanalytical study of accessory and opaque minerals using electron microprobe analysis. Except for one sample from drill hole 42 (to study the hydrothermal sulfide mineralization in suevites), all samples were taken from drill holes 50 and 11475. Thin sections of these impact melt rock samples were studied with optical microscopy to select representative assemblages and measurement points for EMPA. Rock-forming minerals, their generations, and the order of crystallization, on one hand, and the crystalline or glassy state of the matrix, on the other hand, were used as the main petrographic criteria for the selection of the main varieties of impact melt rocks for electron microprobe analyses of accessory minerals contained therein. From

the lower unit, impact melt rocks were sampled from drill holes 50 (intervals 734 and 667 m) and 11475 (intervals 778, 775, 761, 694, and 669 m), see Fig. 2. From the upper unit, crystalline impact melt rocks were sampled from drill holes 50 (intervals 652, 650, 603, and 598 m) and 11475 (interval 605 m), see Fig. 2.

Investigations of the chemical composition, crystal habit, and microtexture of the accessory and opaque minerals from impact melt rocks of the Boltysh structure were performed using a scanning electron microscope JEOL JSM-6490LV and an INCA Energy$^+$ X-ray spectrometry system (Oxford Instruments).

The system was composed of an energy dispersive spectrometer (EDS) INCAx-act with an analytical silicon drift detector (ADD), a wavelength dispersive spectrometer (WDS) INCA Wave 500, and program that allows EDS and WDS analyses to be carried out separately or simultaneously.

The investigations were fulfilled in the regime of backscattered electron images (BSE). The acceleration voltage of the EDS analysis was 20 kV, and the beam current was 1–1.5 nA. The WDS analyses were carried out at an acceleration voltage of 20 kV and beam current of 25–30 nA. The resolving capacity of the EDS was <133 eV, and the capacity of the WDS was 5–10 eV. The detection limits were <0.2 wt% of the EDS and <0.01 wt % of the WDS. Peak counting time was 30 s for the biggest part of elements measured. The background was evaluated for 15 s on either side of each peak. The universal collection of 55 elements for X-ray microanalysis (Micro-Analysis Consultants Ltd., Cambridgeshire PE27 3LF UK) was used for the calibration of the analytical program Oxford INCA Energy$^+$.

RESULTS

Native Metals and Alloys

Native metals in the impact melt rocks of the Boltysh structure are copper, platinum, silver, and gold. All these minerals, except the last, occur in the impact melt rock of the upper unit together with chloritized pyroxene (drill hole 50, 650 m), whereas gold, natural brass (Cu-Zn alloy), and silver-copper alloys were discovered in the impact melt rock of the lower unit.

Native copper is present in the form of vein-like segregations and irregular grains that occur at the contacts of chlorite and feldspar microliths within the matrix. Locally, they are observed in fissures in the groundmass of the melt rock. The thickness of the copper veins varies from 1–2 to 10–15 μm, and their length reaches up to 100–150 μm (Fig. 4a). The Cu content is ~96–99 wt%, measured in several grains (Table 1, samples 11, D–3). The main admixture in their composition is Fe, the concentration of which reaches up to 3 wt% in some grains. Inclusions of native platinum locally occur in copper. The only grain of silver, 1 × 3 μm in size, was found in a copper segregation.

Native platinum was observed in the microcrystalline melt rock together with native copper. It forms individual grains of irregular shape (micronuggets), more rarely vein-like segregations in the melt matrix (Fig. 4b). In some places, platinum grains form inclusions in native copper (Fig. 4c). The size of the platinum grains ranges between 2 × 3 and 3 × 8 μm. With a Pt content of up to 99 wt%, this phase is essentially pure Pt; the remaining constituents are Fe (up to 2.2 wt%), Cu (up to 2.2 wt%), and Si (up to 0.7 wt%) (Table 1, samples 67, H–3).

Cuproplatinum (Betechtin 1935; Mineraly 1960) is present as individual grains of irregular shape in the same rock sample of the upper unit that also contains platinum. The grains and aggregates of cuproplatinum are homogeneous and do not show any traces of decomposition. The composition of this phase is 80–85 wt% Pt, 12–15 wt% Cu, and to 1.8 wt% Fe (Table 1, sample 52).

Native silver was detected in the impact melt rock of the upper unit together with native copper and platinum. Silver is present in segregations of irregular shape, but it also forms veins and vein-like structures. The veins of native silver usually occur at the contacts of chlorite and feldspar microliths with the melt matrix, and rarely spread into the cryptocrystalline matrix (Fig. 4d). The silver grains and aggregates range in size from several micrometers to about 20 μm, whereas silver veins rarely reach 50–60 μm in length. The concentration of Ag is 95–99 wt% (Table 1, samples D-6, 68). The remaining constituents are Fe and Si, but for the latter the surrounding matrix is considered to be its possible source.

Only one grain of native gold was discovered in an impact melt rock with a glassy matrix (drill hole 11475, 761 m). The grain is oval shaped and 1.3 × 2.1 μm in size. The content of Au is 92.6 wt%; the remaining constituents are 1.2 wt% Fe and 0.9 wt% Cu. The presence of Si, Al, and oxygen is probably due to the influence of the surrounding matrix.

Five grains of copper-zinc alloy (natural brass) were encountered in the impact melt rock of the lower unit (drill hole 11475, 761 m). All grains have irregular shapes and sizes from 2 × 3 μm to 7 × 15 μm (Fig. 4e). Zn content is 35.8–37.5 wt% (Table 1, samples 42, 43). The atomic ratio of Cu to Zn is nearly constant and ranges between 1.7:1 and 1.8:1.

A single droplet-shaped grain of a natural silver-copper alloy, 7 × 9 μm in size, was found in the impact

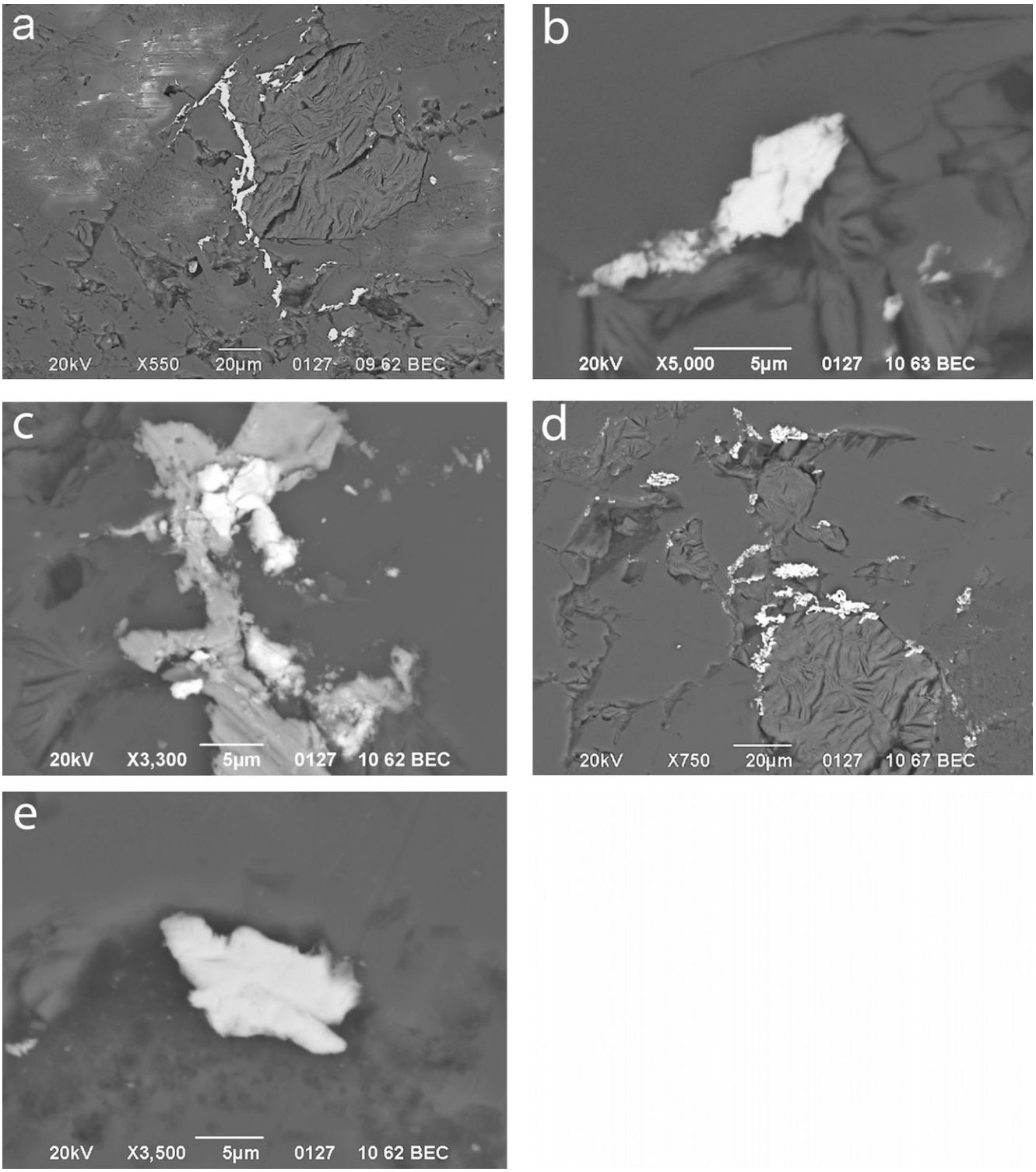

Fig. 4. Native metals and natural brass in impact melt rocks of the Boltysh structure (BSE images). a) A vein of native copper (white) at the boundary of secondary chlorite filling (right, with the "wrinkly" surface) and matrix. b) Veinlets of native platinum (white) at the boundary of chlorite and matrix. c) Grains of native platinum (white) in veinlets of copper (light gray). d) Veinlets and irregular segregations of native silver (white) located predominantly around a chlorite grain (a–c: drill hole 50, 650 m). e) An irregularly shaped grain of natural brass in glassy matrix (drill hole 11475, 761 m).

Table 1. Electron microprobe analyses (EDS data, the low contents of Pt, Os, Au, Ag, Ni, Cu, and Zn in samples D-3, 67, H-3, 52, D-6, 68, 42, and 43—WDS data) of native metals and natural brass from impact melt rocks of the Boltysh structure.

Sample	Cu 11	Cu D-3	Pt 67	Pt H-3	Cu-Pt 52	Ag D-6	Ag 68	Cu-Zn 42	Cu-Zn 43
Cu	97.3	99.2	–	0.6	12.3	–	–	60.3	61.9
Ag	n.d.	n.d.	n.d.	–	n.d.	99.9	100.6	n.d.	n.d.
Au	n.d.	n.d.	n.d.	–	n.d.	–	n.d.	n.d.	–
Fe	2.4	0.4	1.0	1.2	1.8	0.7	–	–	–
Ni	n.d.	n.d.	n.d.	–	n.d.	–	n.d.	–	–
Zn	n.d.	n.d.	n.d.	–	n.d.	–	n.d.	35.8	37.5
Pt	n.d.	–	99.0	96.5	86.4	–	–	n.d.	–
Os	n.d.	–	–	–	–	–	–	n.d.	–
Si	–	0.6	–	0.7	–	–	0.4	–	0.4
Total	99.7	100.2	100.0	99.0	100.5	100.6	101.0	96.1	99.8

Samples: 11, D-3, 67, H-3, 52, D-6, 68—borehole 50, depth 650 m; samples 42 and 43—borehole 11475, depth 761 m.
n.d. = not determined; – = lower detection limit.

melt rock with copper-zinc alloy. The major constituents of this phase are Ag (72.4 wt%) and Cu (26.8 wt%). However, 1.1 wt% of Si is attributed to the influence of the surrounding matrix.

Oxides in Impact Melt Rocks of the Boltysh Structure

Accessory oxides in the impact melt rocks of the Boltysh structure are ilmenite, hematite, Fe–Ti oxide, and baddeleyite.

Ilmenite occurs in all types of impact melt rocks investigated in this study. It forms tabular crystallites and irregular grains up to 50–70 μm in size. The mineral occurs in the melt matrix and locally forms intergrowths with orthopyroxene microliths (Fig. 5a). The growth of orthopyroxene on the ilmenite crystals indicates that ilmenite crystallized prior to orthopyroxene.

The composition of ilmenite in the impact melt rocks of the lower unit is in good agreement with the theoretical stoichiometric formula of the mineral (Table 2, samples 3, 4). However, ilmenite from the upper unit often shows a slight deficit of titanium and contains several percent by weight of Fe_2O_3 (Table 2, sample 5). Furthermore, these ilmenites contain up to 2.0 wt% MgO, 0.6 wt% MnO, 0.1 wt% NiO, and 0.1 wt% CoO. Two ilmenite grains analyzed contain 0.2 wt% and 0.3 wt% of ZrO_2.

Varieties of hematite with high contents of TiO_2, Al_2O_3, and Cr_2O_3 are present in the impact melt rocks of the Boltysh structure. Hematite with a high content of TiO_2 was found in the impact melt rock from the upper unit of drill hole 50 (interval 650 m). The mineral forms subhedral, rarely spherulitic, grains between 3–5 to 30 μm in size (Fig. 5b). All grains appear texturally homogeneous and do not contain any visible traces of decomposition. The majority of the Fe in the mineral was determined as Fe^{3+} on the basis of the number of oxygen atoms after saturation of all other monovalent cations with oxygen (Reed 2005). The main peculiarity of the mineral composition is high TiO_2 content, i.e., from 14.9 up to 16.2 wt% (Table 3, samples 9, 33). The content of Al_2O_3 in the mineral is from 3.3 up to 5.4 wt%. The formula of the analyzed mineral shows its conformity to hematite with the sum of cations from 3.9 to 4.0.

Rare grains of hematite with lower contents of TiO_2 (6.2 wt%) and Al_2O_3 (3.9 wt%) were also found in a sample of the glassy impact melt rock from drill hole 50 (interval 734 m).

A variety of hematite with high contents of Al_2O_3, Cr_2O_3, and TiO_2, was discovered in the upper unit of the impact melt sheet in drill hole 50 (interval 598 m). This variety occurs in the impact melt rock of the upper unit. It forms short-prismatic crystallites some 5–30 μm in size. The composition of this hematite variety is characterized by high contents of Al_2O_3 (6.7–9.3 wt%), TiO_2 (3.6–6.3 wt %), Cr_2O_3 (3.8–8.6 wt%), and V_2O_3 (up to 1 wt%); see Table 3, samples 8, 11.

A Fe-Ti oxide was discovered in the glassy impact melt rocks of the lower unit (drill hole 11475, 775 and 778 m). It forms euhedral prismatic crystals between 10 × 20 and 20 × 60 μm in size embedded in a glassy matrix; intergrowths with other phases were not observed (Figs. 5c and 5d). This mineral is homogeneous and does not exhibit any traces of disintegration. According to calculation of cations by oxygen (Reed 2005), iron in its composition is represented by Fe^{2+}. Its major constituents are FeO (71.7–73.4 wt%) and TiO_2 (21.2–23.4 wt%); additionally, limited amounts of Al_2O_3 (up to 0.8 wt%), MgO (2.4 wt%), and V_2O_3 (up to 0.8 wt%) were also determined (Table 4).

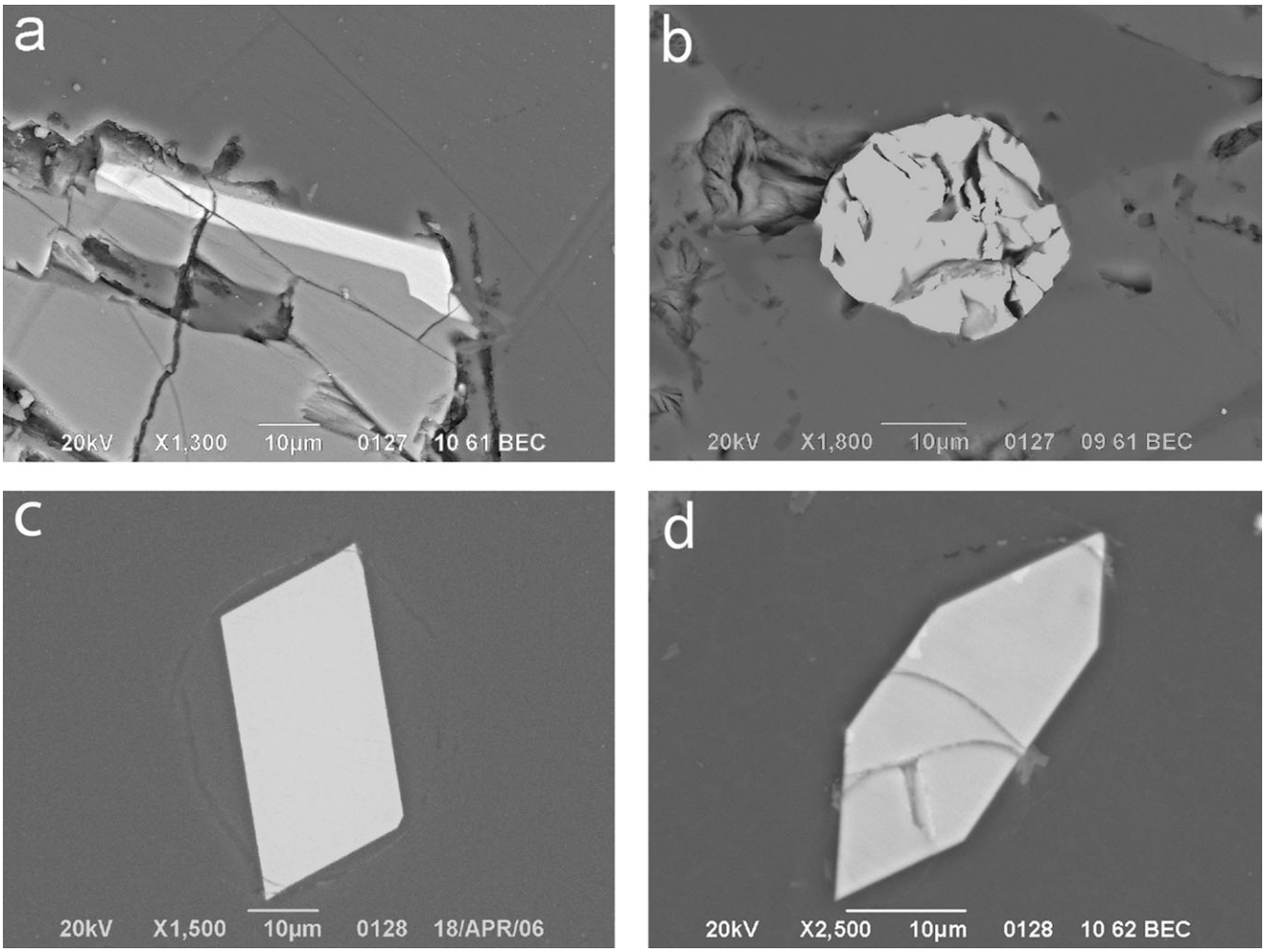

Fig. 5. Iron and titanium oxides in impact melt rocks of the Boltysh structure (BSE images). a) A tabular crystal of ilmenite (white) between orthopyroxene (light gray) and glassy matrix (dark gray) (drill hole 11475, 778 m). b) An irregular grain of titanohematite in matrix (drill hole 50, 650 m). c–d) Prismatic crystals of a preliminarily determined Fe–Ti oxide in glassy matrix (drill hole 11475, 778 m).

Baddeleyite is a rare accessory mineral that forms euhedral prismatic and tabular crystallites up to 20 μm length (Figs. 6a and 6b). Remnants of zircon were not observed in the intergrowths with the baddeleyite crystals. Only one aggregate of irregular oblong baddeleyite grains was observed in the rock of the upper unit. The size of the complex-structured aggregate is about 20 μm, and the size of the individual grains reaches up to 5 × 15 μm (Fig. 6c). The composition of baddeleyite corresponds to zirconium oxide with ZrO_2 content up to 94.7 wt% and lower concentrations of HfO_2, TiO_2, and Fe_2O_3 (Table 5, samples 6, 25).

Sulfides in Impact Melt Rocks of the Boltysh Structure

Sulfides in impact melt rocks are represented by pyrrhotite, pyrite, and sphalerite.

Although pyrrhotite and its Cu- and Ni-rich varieties are widespread accessory minerals in the glassy impact melt rocks of the lower unit, they were not observed in the microcrystalline impact melt rocks. Segregations of pyrrhotite occur in a glassy matrix and rarely form inclusions in microliths of orthopyroxene. In places, radially oriented spinifex-textured quench crystals of orthopyroxene form aureoles around pyrrhotite spheres (Fig. 7a). This spatial arrangement of pyrrhotite and trichites strongly suggests that the pyroxenes formed after the sulfide phase. Pyrrhotite also occurs in the form of hexagonal tabular crystallites, 2–10 μm in diameter (Fig. 7b), but spheres 4–30 μm in diameter are predominant. The heterogeneous structure of some pyrrhotite spheres with lighter and darker (in BSA mode) areas of irregular shapes is visible in the images (Figs. 7c and 7d).

Table 2. Electron microprobe analyses (EDS data) of ilmenite from impact melt rocks of the Boltysh structure.

Hole	11475	11475	50
Depth (m)	778	778	603
Sample	3	4	5
SiO_2	–	–	0.9
TiO_2	52.7	53.0	50.1
Fe_2O_3	–	–	4.2
FeO	44.8	44.7	44.5
MnO	0.5	0.6	0.6
MgO	2.0	1.7	–
Total	100.0	100.0	100.3
Number of cations calculated on the basis of six oxygen atoms			
Ti	1.98	1.99	1.89
Fe^{3+}			0.16
Fe^{2+}	1.87	1.87	1.87
Mn	0.02	0.02	0.03
Mg	0.15	0.13	
Total	4.02	4.01	3.95

– = lower detection limit.

Table 3. Electron microprobe analyses (EDS data) of Ti-hematite (samples 9 and 33) and Al-Ti-Cr-hematite (samples 8 and 11).

Drillhole	50		50	
Depth (m)	650		598	
Sample	9	33	8	11
Fe_2O_3	78.2	81.0	81.0	81.8
Cr_2O_3	–	–	4.7	4.2
V_2O_3	0.6	–	0.7	1.0
MgO	1.1	–	–	–
Al_2O_3	5.4	4.4	7.2	6.7
TiO_2	14.9	15.0	6.2	5.5
Total	100.2	100.4	99.8	99.2
Number of cations on the basis of six oxygen atoms				
Fe^{3+}	2.91	3.09	3.04	3.11
Mg	0.08			
Cr			0.18	0.17
V	0.02		0.02	0.03
Al	0.31	0.26	0.42	0.40
Ti	0.56	0.57	0.23	0.21
Total	3.88	3.92	3.89	3.92

– = lower detection limit.

Pyrrhotites with a low content of isomorphous admixtures are abundant. They are present as individual grains, but more frequently they form predominant parts of complex spheres with some areas enriched by Ni and Cu. The composition of pure pyrrhotite corresponds to the stoichiometric formula of the mineral with a slight deficit of Fe, i.e., $Fe_{0.86–0.88}S_{1.00}$ (Table 6, samples P–5, 8, C–19, P–2).

The contents of Cu and Ni are variable in pyrrhotite spheres and reach up to 30 wt% of both Cu and Ni in some areas within the spheres. While the Cu content is lower than 0.1 wt% in most of the spheres investigated, some areas with Cu contents of up to 10–20 wt% and higher were found (Table 6, samples 26, P–11). An elemental distribution map of two spheres is shown as an example to help visualize the variable content of Cu in pyrrhotite (Fig. 7f). The composition of one area in the sphere with a Cu concentration of up to 30.9 wt% is close to the composition of chalcopyrite: $(Cu_{0.84}Fe_{0.97}Ni_{0.05})_{1.86}S_{2.00}$ (Table 6, sample 8).

The concentration of Ni in pyrrhotites is also highly variable: it ranges from 0 to 20–30 wt% (Table 6, samples 8–3, 8–2, P–1). The areas enriched in Ni in some spheres appear in BSE images as light areas, irregularly outlined and often without sharp margins, surrounded by pyrrhotite with low Ni content (Figs. 7d and 7g). The composition of some areas and zones in pyrrhotite corresponds to the calculated formulas, for example, $(Fe_{0.88}Ni_{0.06}Cu_{0.01})_{0.95}S_{1.00}$, $(Fe_{0.58}Ni_{0.35}Cu_{0.02})_{0.95}S_{1.00}$. The composition of one analyzed pyrrhotite domain with a Ni content of 30.7 wt% nearly corresponds to pentlandite characterized by the formula: $(Ni_{3.74}Fe0_{4.31})_{8.05}S_{8.00}$ (Table 6, sample 13). The content of Co in pyrrhotite reaches 0.1 wt%.

Pyrite was discovered in the upper part of the impact melt sheet. Flat crystals of pyrite, 0.2–2.0 mm in diameter (Fig. 8a), occur in open cracks in the impact melt rock (drill hole 50, 605 m). The pyrite crystals are homogeneous but contain rare inclusions of quartz of up to 50 μm in diameter. Common minor components are up to 0.1–0.2 wt% Ni and Co (Table 7, samples 7, 11).

Veins and irregular segregations of pyrite up to 0.5 mm thick occur in suevites 0.3 m above their lower contact with the melt sheet in drill hole 42, depth 596 m. Complex, zoned, sphere-like composite aggregates some 200 μm in diameter have ~20–30 μm pyrite coating that surrounds cores of cryptocrystalline pyrite and apatite intergrowths (Fig. 8b). In these intergrowths, pyrite forms second-generation cement around apatite grains, about 5–10 μm in size. Analyses of pyrite closely correspond to its theoretical composition (Table 7, samples 2, 12).

Sphalerite rarely occurs in all types of impact melt rocks of the Boltysh structure. It forms irregular grains and aggregates up to 30 μm in size. A chalcopyrite grain, about 3 × 4 μm, was observed in one sphalerite grain. The composition of sphalerite shows that the main admixture in it is 4–5 wt% of Fe (Table 8). The FeS content in the mineral is about 8–10 mol%. The Cu content in sphalerite is as high as ≤0.1 wt% in some grains.

Rare micrometer-sized grains of galenite, chalcopyrite, and acantite occur in the crystalline impact melt rocks of the Boltysh structure.

Table 4. Electron microprobe analyses (EDS data) of Fe–Ti oxide mineral.

Drillhole	11475			11475		
Depth (m)	775			778		
Sample	3	14	1-1	1-1.2	5-2	5-4
TiO_2	21.2	21.9	22.1	22.8	23.1	23.4
Al_2O_3	3.0	3.3	3.4	3.5	3.7	3.0
V_2O_3	1.0	0.4	0.8	n.d.	n.d.	n.d.
Cr_2O_3	–	0.1	n.d.	0.1	n.d.	n.d.
FeO	71.7	72.2	73.4	72.6	73.2	72.5
MgO	1.8	2.0	1.2	2.4	2.1	2.4
NiO	n.d.	0.1	n.d.	0.2	n.d	n.d.
CoO	n.d.	0.1	n.d.	0.1	n.d	n.d.
Total	98.7	100.1	100.9	101.7	102.1	101.3
Number of cations on the basis of five oxygen atoms						
Ti	0.79	0.80	0.80	0.83	0.83	0.83
Al	0.17	0.19	0.19	0.21	0.21	0.17
V	0.03	0.01	0.03			
Cr		0.01		0.01		
Fe^{2+}	2.95	2.94	2.96	2.96	2.93	2.87
Mg	0.13	0.14	0.08	0.17	0.15	0.19
Ni		0.01		0.01		
Co				0.01		
(Fe^{2+},Mg):(Ti,Al,V,Cr)	3.08:0.99	3.09:1.01	3.04:1.02	3.15:1.05	3.08:1.04	3.06:1.00
Total	4.07	4.10	4.06	4.20	4.12	4.06

n.d. = not determined; – = lower detection limit.

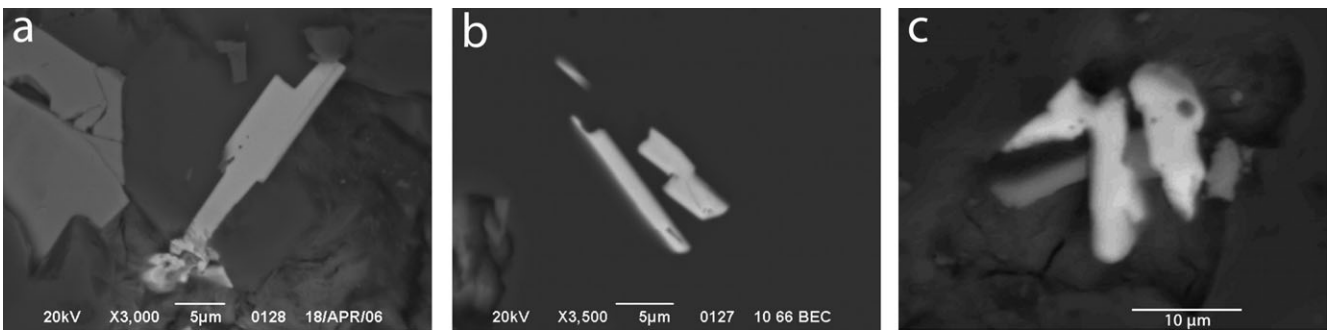

Fig. 6. Baddeleyite in impact melt rocks of the Boltysh structure (BSE images). a) Prismatic crystal of baddeleyite (light gray) in a devitrified glassy matrix (dark gray). Crystal of hypersthene (medium gray) in the left part of the image (drill hole 11475, 694 m). b) Tabular crystallites of baddeleyite in a matrix of crystalline impact melt rock (drill hole 50, 650 m). c) Aggregate of irregular grains of baddeleyite in a cryptocrystalline matrix (drill hole 50, 603 m).

Phosphates in Impact Melt Rocks of the Boltysh Structure

Monazite is the most abundant accessory phosphate in impact melt rocks of the Boltysh crater. It occurs in both types of impact melt rocks. Crystal shapes of monazite from the upper unit range from euhedral tabular crystallites to flattened spheres and irregular grains (Figs. 9a and 9b). They are dispersed in the matrix of the rocks, and in places grains are found in contact with chlorite. In the glassy impact melt rocks of the lower unit, monazite forms euhedral- to subhedral-tabular and thin-tabular crystallites in matrix (Fig. 9c). Furthermore, based on a textural relationship between monazite and pyroxene, it must be concluded that monazite crystallized before pyroxene (Fig. 9d). The size of the monazite crystallites and grains in both rock types is from 2–3 μm to 10–12 μm and reaches up to 20 μm in length in the case of some prismatic crystallites.

In rocks of the lower unit, monazite is characterized by a high Ce_2O_3 content of up to 31.1 wt% together with a high La_2O_3 content of up to 15.2 wt%. Furthermore, the Nd_2O_3 content reaches up to

10.1 wt%, whereas the remaining REE are below the detected limit (Table 9, sample 12). Thus, the REE content decreases in the order: Ce>La>Nd. The concentrations of Th in these monazites range from 1.5 to 4.0 wt%. On the contrary, monazite in the crystalline rocks of the upper unit is characterized by significantly low Ce_2O_3 and La_2O_3 contents (up to 23.9 wt% and 8.7 wt% respectively; see Table 9, samples D–C–3 and 7), and REE contents decrease in the order Ce > Nd > La > Pr > Sm. Moreover, these monazite grains are characterized by high ThO_2 content up to 24.6 wt%, which characterizes these phase as cheralite (Table 9, sample 7).

Apatite occurs in the pyrite-apatite aggregates in hydrothermal veins observed in the suevites. Irregularly shaped apatite grains up to 10 μm in size are commonly cemented by pyrite.

Table 5. Electron microprobe analyses (EDS data) of baddeleyite (samples 6 and 25) and zircon (samples 14 and 9) from impact melt rocks of the Boltysh structure.*

Drillhole	50	50	11474	11475
Depth (m)	650	603	761	778
Sample	6	25	14	9
ZrO_2	94.7	94.6	67.3	69.7
HfO_2	1.2	0.5	–	0.1
TiO_2	1.2	2.0	–	–
SiO_2	–	–	31.3	30.8
Fe_2O_3	0.8	1.4	–	–
Total	97.9	98.5	98.6	100.6

*Description of zircon, the only silicate accessory mineral, determined in impact melt rocks of the Boltysh structure, is given further.
– = lower detection limit.

Accessory Silicates in Impact Melt Rocks of the Boltysh Structure

Zircon is the only accessory silicate mineral found in the impact melt rocks of the Boltysh structure. It rarely occurs in both types of melt rocks. Grains of zircon were partially resorbed by impact melt, and clastic angular grains of irregular shapes were preserved only within the marginal zones of the melt sheet to about 10 m from its contacts (Fig. 10a). Usually, the mineral occurs as elliptical grains about 5–50 μm in size and appears in

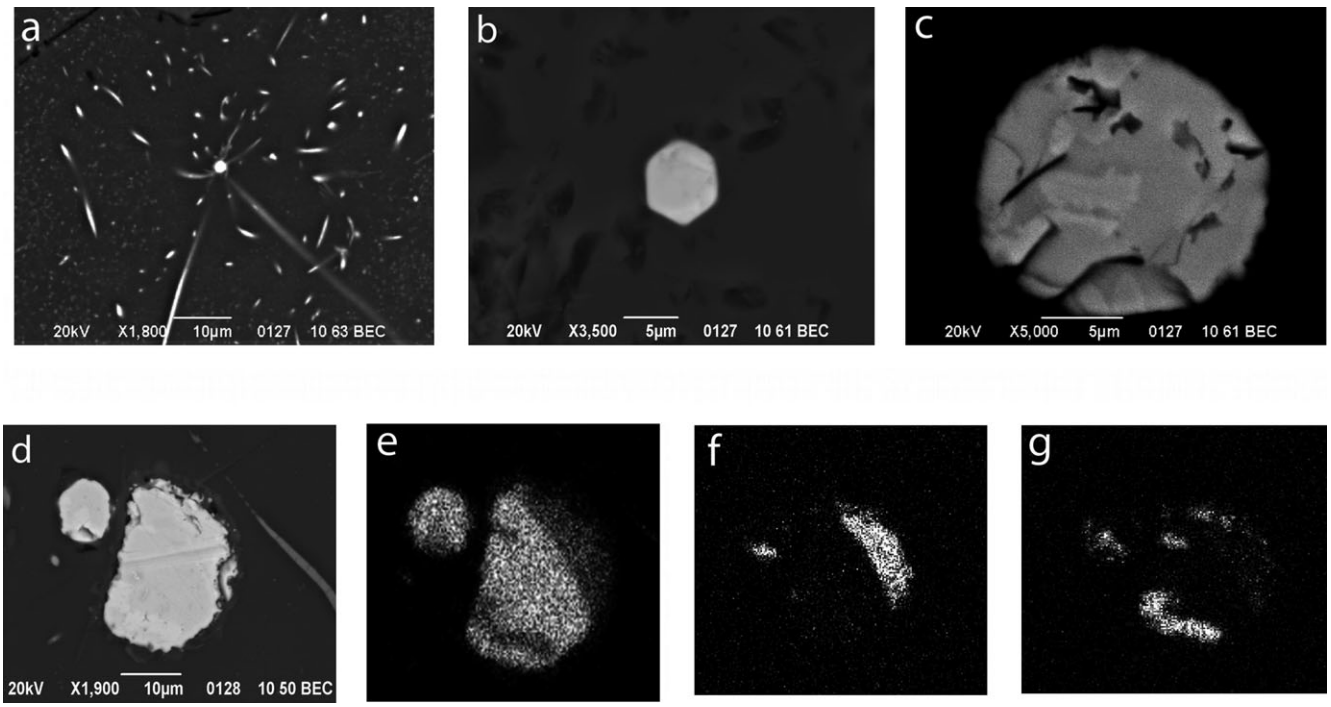

Fig. 7. Pyrrhotite in impact melt rocks of the Boltysh structure (BSE images). a) Sphere of pyrrhotite (bright, in the center) surrounded by rays of spinifex-textured quench crystals of pyroxene (drill hole 50, 664 m). b) Hexagonal crystal of pyrrhotite in a glassy matrix (drill hole 11475, 761 m). c) Sphere of pyrrhotite with high Ni content (12.56–13.34 wt%) in the bright area (drill hole 11475, 761 m). d) Two spheres of Cu- and Ni-bearing pyrrhotite (light gray). The white area in the lower part of the biggest sphere indicates enrichment in Ni domain with a Ni content of 30.70 wt% (drill hole 11475, 761 m). e–g) An elemental distribution maps of the pyrrhotite spheres (d) showing irregular distribution of iron (e), copper (f), and nickel (g) (drill hole 11475, 694 m).

Table 6. Electron microprobe analyses (EDS data, Ni content in analyses C-19, and P-11—WDS data) of pyrrhotite and its Cu– and Ni–rich varieties.

Drillhole	11475	11475	11475	11475	11475	11475	11475	50	50	11475	11475
Depth (m)	761	667	761	761	761	761	694	664	664	667	694
Sample	P-5	8	C-19	P-2	26	P-11	8	8-3	8-2	P-1	13
Fe	59.6	60.5	60.5	60.1	57.9	54.8	30.4	49.3	42.6	37.0	33.6
Ni	–	–	0.1	–	0.3	0.1	1.5	12.3	19.7	23.6	30.7
Cu	–	–	–	–	3.7	6.3	30.9	–	–	1.3	–
S	38.8	40.3	37.3	40.5	37.9	39.0	36.1	37.4	37.2	36.8	35.8
Si	0.5	0.3	0.8	0.6	0.4	0.5	1.4	–	0.3	0.9	0.5
Total	98.9	101.1	98.7	101.2	100.2	100.7	100.3	99.0	99.8	99.6	100.7
Number of cations on the basis of one sulfur atom (analysis 13: eight sulfur atoms)											
Fe	0.88	0.86	0.93	0.85	0.88	0.81	0.48	0.75	0.66	0.58	4.31
Ni					0.00	0.00	0.02	0.18	0.29	0.35	3.74
Cu					0.05	0.08	0.42			0.02	–
Total	0.88	0.86	0.93	0.85	0.93	0.89	0.92	0.93	0.95	0.95	8.05

– = lower detection limit.

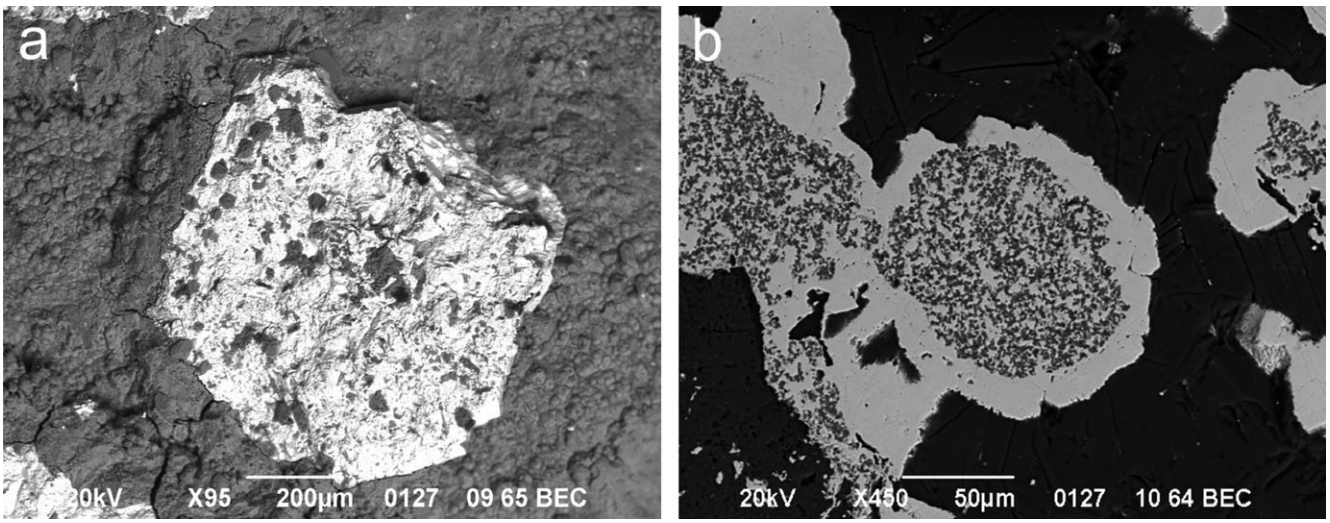

Fig. 8. Pyrite in impact melt rock and suevite of the Boltysh structure (BSE image). a) Aggregation of pyrite on the surface of an open fissure in impact melt rock (drill hole 50, 605 m). b) Complicated aggregates of sulfides and phosphates in suevite: coating of pyrite (white) surround thin-grained aggregates (gray) of pyrite and apatite (drill hole 42, 596 m).

oval sections. Rarely, parallel-oriented planar microstructures are visible in BSE images of some zircons (Fig. 10b). Furthermore, zoned subhedral zircon grains with granular rims occur in the impact melt rocks of the lower unit (Fig. 10c). Resorbed composite grains of zircon were rarely observed in the rocks of the lower unit (Fig. 10d). Compositionally, the measured grains are consistent with the zircon formula. However, some grains show a slight depletion of SiO_2 and an atomic ratio Si to Zr of 0.90–0.95 (Table 5, samples 14, 9).

DISCUSSION AND CONCLUSIONS

An annular sheet of impact melt rocks, 12 km in diameter and up to 220 m thick, is found in the Boltysh impact structure. The accessory minerals in the impact melt rocks are represented by native metals, alloys, oxides, sulfides, phosphates, and silicates, which formed during a wide interval of cooling, solidification, and hydrothermal alteration of the melt sheet and, thus, from the very beginning of crystallization of high-temperature minerals to the formation of native metals and some sulfides during alteration.

Baddeleyite, titanium-ferrous oxides, monazite, pyrrhotite, native brass, and native gold represent minerals crystallized from the liquid phase in a wide temperature interval from about 3000 °C of baddeleyite crystallization (Mineraly 1965) down to complete solidification of the impact melt. The last liquid phase of impact melt after crystallization of microliths of

Table 7. Electron microprobe analyses (EDS data, Ni, Co, and Cr content—WDS data) of pyrite from impact melt rock and suevite of the Boltysh structure.

Drillhole	50	50	42	42
Depth (m)	605	605	596	596
Sample	7	11	2	12
Fe	45.5	46.5	46.7	46.8
Ni	0.08	0.15	–	–
Co	0.07	0.21	0.03	0.03
Cr	–	–	–	0.02
S	55.5	51.4	53.7	53.2
Total	101.15	98.26	100.35	100.05
Atomic proportions				
S:Fe	2.12	2.00	2.00	1.99

– = lower detection limit.

Table 8. Electron microprobe analyses (EDS data, content of Cr, Co, and Cu—WDS data) of sphalerite from impact melt rocks of the Boltysh structure.

Drillhole	50	11475	50	50
Depth (m)	650	694	603	603
Sample	35	12	2	12
Zn	65.7	62.3	60.3	58.9
Fe	–	3.2	4.4	5.3
Cr	n.d.	n.d.	0.04	0.03
Co	n.d.	n.d.	0.02	–
Cu	n.d.	–	0.09	0.10
S	34.1	33.9	35.3	35.2
Total	99.8	99.4	100.15	99.53
Number of cations on the basis of one sulfur atom				
Zn	0.94	0.90	0.84	0.81
Fe		0.05	0.07	0.08

n.d. = not determined; – = lower detection limit.

pyroxene and plagioclase produced the glassy or the cryptocrystalline matrix of the impact melt rocks. The composition of the glassy matrix is close to the composition of granitic eutectic (Grieve et al. 1987; Gurov et al. 2011). This allows researchers to estimate the approximate temperature of solidification of the matrix using experimental investigations of granitic systems. The temperature of solidification of the granite system at a pressure of $P_{H_2O} = 0.5$ kbar is about 780 °C (Tuttle and Bowen 1958), and about 930 °C at a pressure of P_{H_2O}~1 bar (Luth et al. 1964). Thus, the solidus temperature of the matrix of the impact melt rocks at Boltysh may be estimated to approximately 800–900 °C (Fig. 11).

Baddeleyite in impact melt rocks is a product of the decomposition of zircon during stage IV of shock metamorphism at shock pressures in excess of 60 GPa and postshock temperatures in excess of 1500 °C (Stöffler 1971; Wittmann et al. 2006). Baddeleyite in the impact melt rocks of the Boltysh structure occurs as euhedral prismatic and tabular crystals. It is supposed that these particular shapes are evidence for formation from a liquid phase at high temperatures in the order of 2690–3000 °C (Fig. 11) (Mineraly 1965). This may have resulted from the decomposition of zircon and the resultant presence of free ZrO_2 in the impact melt at shock pressures above 60 GPa (Wittmann et al. 2006). Rarely, baddeleyite in impact melt rocks of the Boltysh structure occurs as complex aggregations of irregular grains, formed by the complete granularization and decomposition of zircon without melting. The complete decomposition of zircon was observed in suevites and impact melt rocks of the Ries and other impact craters in shapes of aggregations of irregular micron-sized grains of baddeleyite in a glassy matrix (Wittmann et al. 2006).

Zircon rarely occurs in the impact melt rocks of the Boltysh structure, thus the studied samples do not record all stages of its shock metamorphism. The presence of planar microstructures in some zircon grains bears witness to their shock metamorphism at stages I and II at shock pressures of 20–40 GPa and postshock temperatures up to 900 °C (Stöffler 1971; Erickson et al. 2013). Partial melting and resorption of rounded grains of zircon by impact melt take place at temperatures of about 1900–1700 °C (El Goresy 1964, 1968; Wittmann et al. 2006). Rare composite grains of zircon are the products of granularization known to operate at stages III and IV of shock metamorphism, at postshock temperatures of up to 3000 °C (Wittmann et al. 2006).

Monazite occurs in both units of the impact melt rocks. The crystallization of monazite prior to hypersthene is suggested by the textural relationships between these minerals. The composition of the marginal zones of hypersthene in the impact melt rocks of the Boltysh structure is $En_{40–50}Fs_{50–60}$ (Gurov et al. 2011), which allows the temperatures of its inversion to be calculated in the range of 1000–1050 °C (Bowen and Schairer 1935; Deer et al. 1963). These temperatures indicate that the lower temperature limit of monazite crystallization was about 1100 °C, while the monazite melting point is around 1750 °C (Fig. 11).

Titanohematite is the abundant accessory oxide mineral in the impact melt rocks of the lower unit. The high TiO_2 Al_2O_3 contents in its composition probably indicate high-temperature crystallization. According to experimental data (MacChesney and Muan 1959), hematite is a stable phase of pure Fe oxide up to a temperature of 1390 °C. It transforms to magnetite at higher temperatures, but the presence of 10 wt% TiO_2 extends the hematite stability field to higher temperatures at ~1524 °C (Fig. 11). Al-, Ti-,

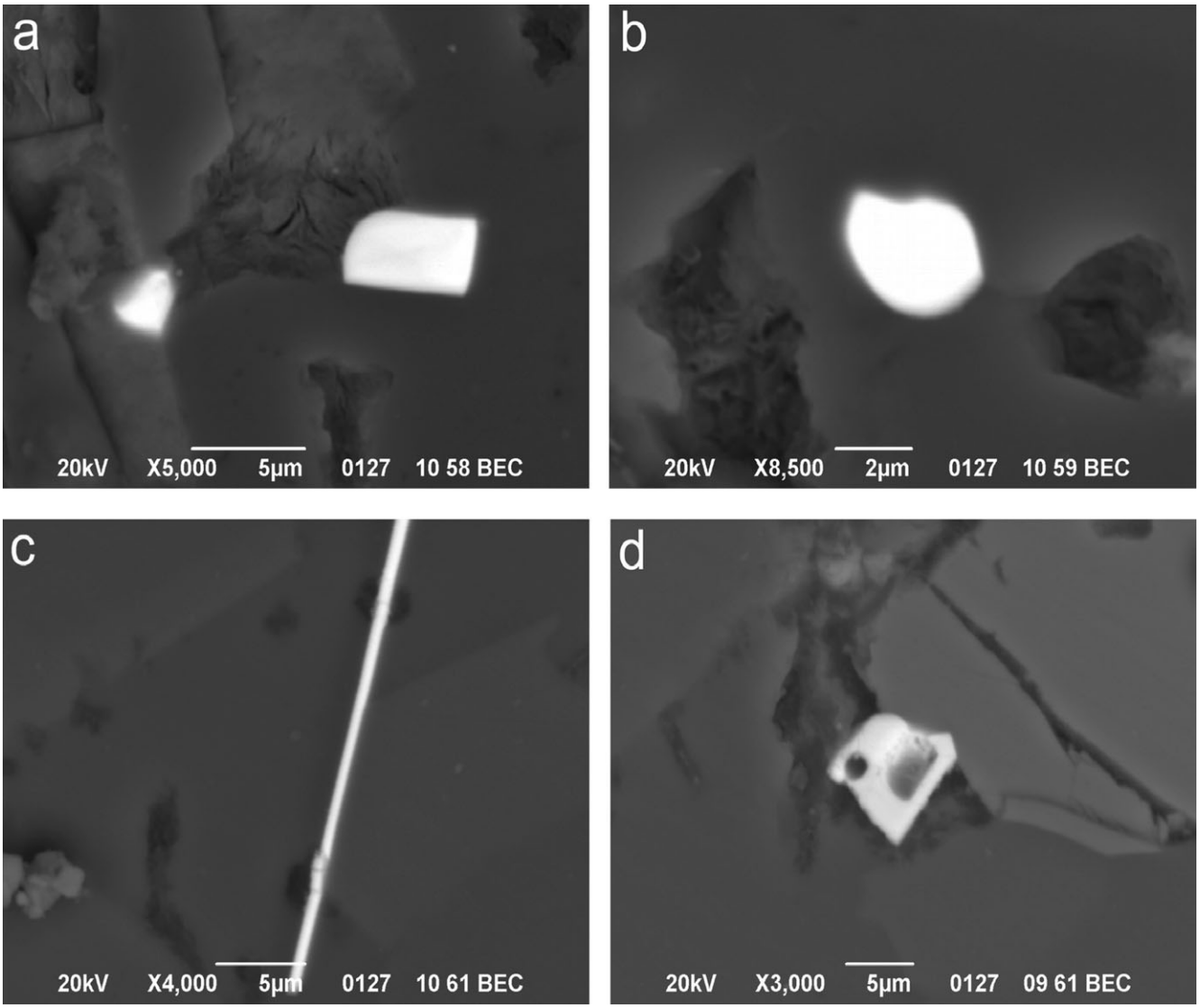

Fig. 9. Monazite in impact melt rocks (BSE images). a) Prismatic crystal of monazite at the contact with chlorite (upper right) (drill hole 50, 603 m). b) Oval grain of monazite in a matrix of crystalline impact melt rock (drill hole 50, 603 m). c) Thin tabular crystallite of monazite in glassy matrix (drill hole 11475, 761 m). d) Contact of subhedral crystal of monazite (white) with pyroxene (dark gray) (drill hole 11475, 761 m).

and Cr-bearing hematite exists in microcrystalline impact melt rock from the upper horizon of the impact melt sheet. The high content of the Al_2O_3 (7–9 wt%) may be explained by the high temperatures during hematite crystallization. A solution of 10 wt% of Al_2O_3 in hematite is achieved at temperatures of about 1300 °C (Muan and Gee 1956; Muan 1957). A peculiarity of the composition of this variety of hematite is the high content of Cr_2O_3, which is up to 8 wt% in some grains.

A Fe-Ti oxide mineral with a TiO_2 content of 21–23 wt% and FeO content of 71–73 wt% was identified in the impact melt rock of the lower unit. Its iron and titanium contents are close to the contents in some titanomagnetites (Deer et al. 1962; Bowles et al. 2011), but the crystal shapes of the mineral do not allow it to be identified as a cubic titanomagnetite or ulvöspinel. Furthermore, the content of TiO_2 is about half the concentration of TiO_2 in pseudobrookite (Mineraly 1967; Bowles et al. 2011). The atomic ratio of iron group elements (Fe^{2+} + Mg) and titanium group elements (Ti + Al + V + Cr) is ~3.0. Thus, the mineral presumably has 5 oxygen atoms. The proposed formula of the mineral is: $(Fe^{2+}, Mg)_{3.0}{\cdot}(Ti, Al, V)_{1.0}{\cdot}O_{5.0}$. We suppose that this might be a new mineral species, which, however, requires further investigation. We note

Table 9. Electron microprobe analyses (EDS data) of monazite (samples 12, D-C-3), and cheralite (sample 7) from impact melt rocks of the Boltysh structure.

Drillhole	11475	50	50
Depth (m)	775	650	650
Sample	12	D-C-3	7
SiO_2	5.5	2.3	2.4
ThO_2	3.9	12.4	24.6
La_2O_3	15.2	8.7	4.3
Ce_2O_3	31.1	23.9	21.6
Pr_2O_3	–	3.0	–
Nd_2O_3	10.1	9.7	7.3
Sm_2O_3	–	1.7	–
Eu_2O_3	–	0.6	–
Gd_2O_3	–	1.6	–
Tb_2O_3	–	0.7	–
Dy_2O_3	–	0.6	–
Fe_2O_3	1.0	1.7	1.3
CaO	0.6	2.3	5.7
P_2O_5	31.2	30.9	31.1
Total	98.6	100.1	98.3

– = lower detection limit.

that still unknown mineral species may exist in the series: $FeO{\cdot}2TiO_2$–$FeO{\cdot}TiO_2$–$2FeO{\cdot}TiO_2$ with a relatively higher content of FeO in relation to titanomagnetite and ulvöspinel, as it was proposed by Deer et al. (1962).

Ilmenite occurs in all rock types of the melt sheet. As inferred from textural relationships with other mineral phases in the melt rocks, it is one of the earliest generations of minerals crystallized before pyroxene. It is supposed that the deficit of TiO_2 in some analyzed ilmenites is balanced by the presence of 4–8 wt% of Fe_2O_3. According to Deer et al. (1962) and Bowles et al. (2011), ilmenite contains Fe^{3+} only at temperatures in excess of 1200 °C (Fig. 11). A high content of Fe_2O_3 in ilmenite was already described (see e.g., El Goresy 1968; Bowles et al. 2011). The admixture of 0.2–0.3 wt% of ZrO_2 was determined in two ilmenite grains. Previously, ZrO_2 in ilmenite was described from lunar basalts only (Frondel 1975). No inherited grains of ilmenite potentially derived from the target rocks were observed in the impact melt rocks of the Boltysh structure, whereas nonfused ilmenite with armalcolite rims has been found in glass from the Ries crater (El Goresy and Chao 1976).

Pyrrhotite, the most abundant accessory sulfide from the impact melt rocks of the lower unit, is the main concentrate for some rare elements, especially Ni and Cu. The composition of this mineral and shape of its crystallites prove that it is a high-temperature hexagonal pyrrhotite (Mineraly 1960; Bowles et al. 2011). According to Deer et al. (1962), the crystallization temperature of pyrrhotite with a sulfur content of 40 wt% reaches a maximum (i.e., 1200 °C) in the system Fe–S. Moreover, pyrrhotite crystallized from the melt before the formation of spinifex-textured quench crystals of eulite with 15–20 mol% enstatite component (Gurov et al. 2011), and these were formed at temperatures of about 950 °C (Bowen and Schairer 1935; Deer et al. 1963). Thus, the temperatures of pyrrhotite crystallization were likely in the range of 1200–950 °C (Fig. 11). Nickel- and Cu-bearing pyrrhotites were described earlier from impact melt rocks and glasses from other terrestrial impact craters (El Goresy 1968; von Engelhardt 1972). For example, sulfide spheres with a Ni content of 25.5 wt% and a Cu content of 26.0 wt% were found in impact glasses of the Ries crater, as described by Stähle (1972). Ni- and Cu-bearing sulfides were found in impact melt rocks from the Morokweng structure (Andreoli et al. 1999).

Native brass and gold occur in the glassy impact melt rocks, but these do not contain any traces of secondary alteration processes. Thus, their crystallization in impact melt is evident. Formation of native gold occurs at a temperature of about 1060 °C (Mineraly 1960), whereas solidification of copper-zinc alloys with Zn contents of about 35–40 wt% takes place at temperatures of about 900 °C (Volkov and Zharskiy 2005). A copper-zinc alloy with 30–45% Zn in lunar basalts was described earlier (Frondel 1975). Later Cu-Zn intermetallic minerals were determined in some ore deposits in China (Xie et al. 2006) and Russia (Akimova et al. 2008).

Formation of native copper, native platinum, cuproplatinum, native silver, pyrite, and sphalerite in the impact melt rocks took place after their complete solidification during cooling and concomitant hydrothermal alteration at temperatures below 800 °C.

Native metals (i.e., copper, silver, platinum, and cuproplatinum) occur within the upper unit of the hydrothermally altered impact melt rocks in the form of veins and vein-like aggregates in the matrix and at the margins of chlorite grains. Although pyrrhotite spheres occur in glassy melt rocks, they were not observed in crystalline rocks of the upper horizon of the impact melt sheet. Thus, it is supposed that pyrrhotite was dissolved during hydrothermal alteration of the upper unit, and served as the source of native metals in its basal section. A similar process regarding the formation of native platinum and cuproplatinum was proposed for the massifs of ultramafic rocks in the Urals due to their hydrothermal alteration; a dispersed sulfide mineralization of the massifs was proposed as the source of native metals (Betechtin 1935; Mineraly 1960).

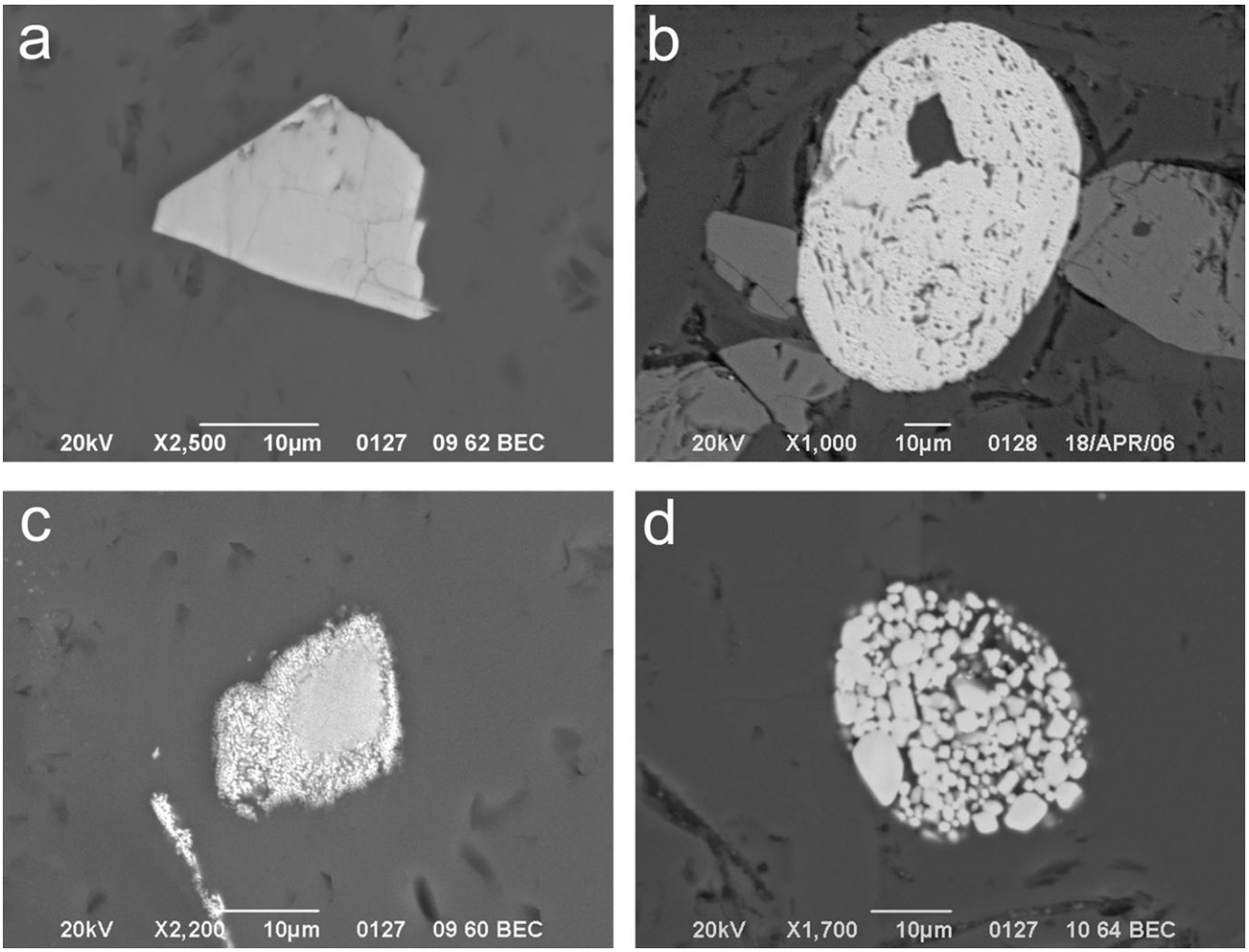

Fig. 10. Zircon in impact melt rocks of the Boltysh structure (BSE images). a) Angular clastic grain of zircon in a glassy matrix (drill hole 50, 734 m). b) Rounded grain of zircon with the remnants of planar microstructures. Gray subhedral crystallites are pyroxene (drill hole 11475, 775 m). c) Zonal grain of zircon with a granular texture (drill hole 50, 734 m). d) Partially dissolved composite grain of zircon in a glassy martix (drill hole 11475, 775 m).

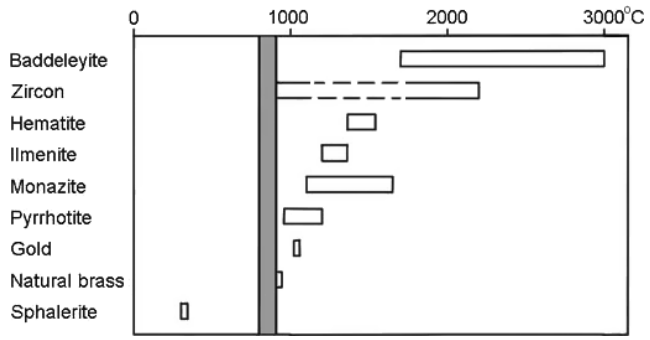

Fig. 11. Schematic diagram of crystallization temperatures of accessory and opaque minerals in the impact melt rocks of the Boltysh structure. Vertical gray band indicates the temperature interval of solidification of the residual melt forming the matrix of the impact melt rocks at 900–800 °C.

Native metals of the PGE are rarely observed in impact melt rocks at terrestrial impact structures. For example, native platinum was described in impact melt rocks with a very high content of projectile matter from the Morokweng structure (Andreoli et al. 1999). Furthermore, subhedral iridium metal grains were identified in melt rocks from the Chicxulub impact structure (Schuraytz et al. 1996). However, the formation conditions of these native metals were not determined in either case.

Sphalerite forms intergrowths with chlorite, which originated during the late low-temperature process of hydrothermal alteration. The content of about 8–10 mol% FeS in sphalerite allows estimation of the crystallization temperature at about 350–300 °C (Kullerud 1953;

Deer et al. 1962). These temperatures are concordant with the temperatures of hydrothermal processes in many impact structures (Naumov 2002, 2005).

The formation of the Boltysh structure by the impact of a chondritic projectile was previously suggested, and the low relative enrichment of impact melt rocks in Ni, Co, Cr, and some PGE has been described (Grieve et al. 1987; Gurov et al., 1986; McDonald et al., 2009). Sulfides, especially pyrrhotite, are the main carriers of the PGE and some other projectile-derived elements in impact melt rocks of the impact structures (Schmidt et al. 1995). Pyrrhotite is the only mineral in the impact melt rocks of the Boltysh structure that contains Ni as a likely component of the projectile. One variety of hematite was determined as a carrier mineral of Cr in the impact melt rocks. Thus, the matter of the projectile was the source of Ni, Cr, Pt, and some other elements in composition of accessory minerals of the Boltysh impact structure, while it is unlikely that the siliceous crystalline rocks of the crater target were the source of these siderophile elements and PGE.

Acknowledgments—This work was funded by the National Academy of Sciences of Ukraine through Project 0111U002103 from 8 June 2010. We are especially grateful to Prof. Dr. W. U. Reimold, Dr. M. Schmieder, and Dr. S. Hamman, whose detailed and very useful comments, reviews, and criticisms of the original manuscript led to considerable improvements not only to the substance of the paper but also to its construction and language. Our great thanks go to A. J. T. Jull and A. P. Baier for their special opinions on our manuscript and efforts to prepare it for publication.

Editorial Handling—Dr. Gordon Osinski

REFERENCES

Akimova A. V., Mokhov A. V., and Plotinskaya O. Ju. 2008. The first occurence of a natural brass at the Bereznyakovsky epithermal gold-ore deposit (South Urals). RMS DPI 2008-2-75-0:238–240. Fedorov session, 2008 (abstracts), Saint-Peterburg, Russia. In Russian.

Andreoli M. A. G., Ashwal L. D., Hart R. J., and Huinzenga J. M. 1999. A Ni- and PGE- enriched quartz norite melt complex in the Late Jurassic Morokweng impact structure, South Africa. *Large impacts and planetary evolution*, edited by Dressler B. O. and Sharpton V. L. *Geological Society of America Special Paper* 339:91–108.

Betechtin A. G. 1935. *Platinum and some other minerals of platinum group*. Moscow: Academy of Sciences of USSR. 148 p. In Russian.

Bowen N. L. and Schairer J. F. 1935. The system MgO—FeO —SiO_2. *American Journal of Science* 29:151–217.

Bowles J. F. W., Howie R. A., Vaughan D. J., and Zussman J. 2011. *Rock-forming minerals, vol. 5A. Non-silicates, oxides, hydroxides and sulphides*. London: The Geological Society. 920 p.

Deer W. A., Howie R. A., and Zussman J. 1962. *Rock-forming minerals, vol. 5. Non-silicates*. Harlow, UK: Longman. 371 p.

Deer W. A., Howie R. A., and Zussman J. 1963. *Rock-forming minerals*, vol. 2. Chain silicates. Harlow, UK: Longman. 406 p.

El Goresy A. 1964. Die Erzmineralien in den Ries- und Bosumtwi Kratergläsern und ihre genetische Deutung. *Geochimica et Cosmochimica Acta* 28:881–892.

El Goresy A. 1968. The opaque minerals in impact glasses. In *Shock metamorphism of natural materials*, edited by Short B. M. and French M. N. Baltimore, Maryland: Mono Book Corp. pp. 531–553.

El Goresy A. and Chao E. C. T. 1976. Identification and significance of armalcolite in the Ries glass. *Earth and Planetary Science Letters* 30:200–208.

Engelhardt W. von. 1972. Shock produced rock glasses from the Ries crater. *Contributions to Mineralogy and Petrology* 36:265–292.

Erickson T. M., Cavosie A. J., Moser D. E., Barker I. R., and Radovan H. A. 2013. Correlating planar microstructures in shocked zircon from the Vredefort Dome at multiple scales: Crystallographic modeling, external and internal imaging, and EBSD structural analysis. *American Mineralogist* 98:53–65.

Frondel J. W. 1975. *Lunar mineralogy*. New York: Wiley-Interscience Publication. 325 p.

Golubev V. A., Karpov G. M., and Popovichenko V. A. 1974. About the meteoritic origin of the Boltysh meteorite-explosion basin at Kirovograd area. *Doklady Academii nauk USSR B* 1:10–13. In Russian.

Grieve R. A. F., Reny G., Gurov E. P., and Ryabenko V. A. 1987. The melt rocks of the Boltysh impact crater, Ukraine, USSR. *Contributions to Mineralogy and Petrology* 96:56–62.

Gurov E. P. and Gurova E. P. 1991. *Geological structure and rock composition of impact structures*. Kiev: Naukova Dumka Press.160 p. In Russian.

Gurov E. P., Kolesov G. M., and Gurova E. P. 1986. Composition of impactites of the Boltysh astrobleme. *Meteoritica* 45:150–155. In Russian.

Gurov E. P., Kelley S. P., and Koeberl C. 2003. Ejecta of the Boltysh impact crater in the Ukrainian Shield. In *Impact markers in the stratigraphic record*, edited by Koeberl C. and Martinez–Ruiz F. Berlin: Springer. pp. 179–202.

Gurov E. P., Kelley S. P., and Koeberl C. 2006. Sediments and impact rock filling the Boltysh impact crater. In *Biological processes associated with impact events*, edited by Cockell C., Koeberl C., and Gilmour I. Berlin: Springer. pp. 335–338.

Gurov E. P., Shekhunova S. B., and Permiakov V. V. 2011. The Boltysh impact structure and its impact melt rocks. *Geofizicheskiy Zhurnal* 33:66–89. In Russian.

Jolley D. W., Gilmour I., Gurov E., Kelley S. P., and Watson J. 2010. Two large meteorite impacts at the K/Pg boundary. *Geology* 38:835–838.

Jourdan F., Reimold W. U., and Deutsch A. 2012. Dating terrestrial impact structures. *Elements* 8:49–53.

Kelley S. P. and Gurov E. P. 2002. Boltysh, another end-Cretaceous impact. *Meteoritics & Planetary Science* 37:1031–1043.

Kullerud G. 1953. The FeS–ZnS system: A geological thermometer. *Norsk Geologisk Tidsskrift* 32:61–147.

Luth W. C., Janes R. H., and Tuttle O. F. 1964. The granite system at pressures of 4 to 10 kbars. *Journal of Geophysical Research* 69:759–773.

MacChesney J. B. and Muan A. 1959. Studies in the system Fe oxide–titanium oxide. *American Mineralogist* 44:926–945.

Masaitis V. L. 1973. *The geological consequences of fall of the crater–forming meteorites*. Leningrad: Nedra. 17 p. In Russian.

Masaitis V. L., Danilin A. N., Mashchak M. S., Raykhlin A. I., Selivanovskaya T. V., and Shadenkov Y. M. 1980. *The geology of astroblemes*. Leningrad: Nedra. 231 p. In Russian.

McDonald I., Koeberl C., and Gurov E. 2009. A meteorite component in melt rocks from the Boltysh impact structure, Ukraine: First assessment (abstract #1252). 40th Lunar and Planetary Science Conference. CD-ROM.

Mineraly. 1960. *Native elements, intrametallic compounds, carbides, nitrides, phosphides, arsenides, antimonides, bismutides, sulfides, selenides, tellurides. Spravochnik*. *Vol. 1*. Moscow: Academia Nauk SSSR. 618 p. In Russian.

Mineraly. 1965. *Simple oxides. Spravochnik*. *Vol. 2, issue 2*. Moscow: Academia Nauk SSSR 343 p. In Russian.

Mineraly. 1967. *Complex oxides, titanates, niobates, tantalates, antimonates, hydroxides. Spravochnik*. *Vol. 2, issue 3*. Moscow: Academia Nauk SSSR. 676 p. In, Russian.

Muan A. 1957. Phase equilibrium relationships at liquidus temperatures in the system $FeO–Fe_2O_3–Al_2O_3–SiO_2$. *Journal of the American Ceramic Society* 40:420–431.

Muan A. and Gee C. L. 1956. Phase equilibrium studies in the system iron oxide–Al_2O_3 in air and at 1 atm.O_2 pressure. *Journal of the American Ceramic Society* 39:207–214.

Naumov M. V. 2002. Impact-generated hydrothermal systems: Data from Popigai, Kara, and Puchezh-Katunki impact structures. In *Impacts in precambrian shields*, edited by Plado J. and Pesonen L. J. Berlin: Springer. pp. 117–171.

Naumov M. V. 2005. Principal features of impact–generated hydrothermal circulation systems: Mineralogical and geochemical evidence. *Geofluids* 5:165–184.

Reed S. J. B. 2005. *Electron microscopic analysis and scanning electron microscopy in geology*. Cambridge, UK: Cambridge University Press. 232 p.

Schmidt G., Palme H., and Kratz K. L. 1995. The fractionation of highly siderophile elements (HSE) in impact melts and determination of the meteoritic components. *Meteoritics* 30:573–574.

Schuraytz B. C., Lindstrom D. J., Marin L. E., Martinez R. R., Mittlefehldt D. W., Sharpton V. L., and Wentworth S. J. 1996. Iridium metal in Chicxulub impact melt: Forensic chemistry on the K/T smoking gun. *Science* 271:1573–1576.

Stähle V. 1972. Impact glasses from the suevite of the Nördlinger Ries. *Earth and Planetary Science Letters* 17:275–293.

Stöffler D. 1971. Progressive metamorphism and classification of shocked and brecciated crystalline rocks at impact craters. *Journal of Geophysical Research* 76:5541–5551.

Tuttle O. F. and Bowen N. L. 1958. Origin of granite in the light of experimental studies in the system $NaAlSi_3O_8–KAlSi_3O_8–SiO_2–H_2O$. *Geological Society of America Memoir* 74:153.

Valter A. A. and Ryabenko V. A. 1977. *Explosion craters of the Ukrainian Shield*. Kiev: Naukova Dumka Press. 154 p. In Russian.

Volkov A. I. and Zharskiy I. M. 2005. *Bol'shoy khimicheskiy spravochnikc*. Minsk: Sovetskaya shckola. 608 p. In Russian.

Wittmann A., Kenkmann T., Schmitt R. T., and Stöffler D. 2006. Shock-metamorphosed zircon in terrestrial impact craters. *Meteoritics & Planetary Science* 41:433–454.

Xie Y., Hou Z., Xu J., Yuan Z., Bai G., and Li X. 2006. Discovery of Cu-Zn, Cu-Sn intermetallic minerals and its significance for genesis of the Mianning-Dechang REE Metallogenic Belt, Sichuan Province, China. *Science of China: Series D* 49:597–603.

Yurk Y. Y., Yeremenko G. K., and Polkanov Y. A. 1975. The Boltysh basin—A buried meteoritic crater. *Sovetskaya geologiya* 2:138–144. In Russian.